A MEMS pressure sensor using electrostatic levitation

Mohammad Mousavi, Mohammad Alzgool, Shahrzad Towfighian

***Abstract*— Applying electrostatic levitation force to the initially-closed gap-closing electrodes of our micro-electro-mechanical system (MEMS) creates multi actuation mechanisms, and opens a new world to the MEMS applications. Electrostatic levitation allows us to measure physical quantities, such as air pressure, by exploiting pull-in instability and releasing. The beam starts from a pulled-in position by applying a voltage difference between two gap-closing electrodes. When enough voltage is applied to the side electrodes, the cantilever beam is released. At the release instant, electrostatic forces, restoring force, and surface force are applied to the cantilever. According to the experimental results of this work, the surface interaction force varies as the pressure changes. This work shows that at the release instant, we can correlate the pressure and the interaction force. This idea is exhibited by two mechanisms in this work: a pressure sensor and a pressure switch. Having side electrodes has enabled measuring interaction forces, which was not possible with conventional gap-closing electrodes. The interaction forces are estimated using the experimental data at different pressures. The results show that the interaction force is mostly repulsive and is increased as the pressure is increased. In addition, we found that the potential voltage between the gap-closing electrodes in pulled-in position immensely influences the surface interactions.**

***Index Terms*— MEMS, pressure sensor, switch, electrostatic levitation**

I. Introduction

The trend of miniaturization for the Internet of Things encourages the development of MEMS-scale sensors, including pressure sensors. The importance of these sensors arises from their usefullness to numerous aspects of life. Devices that track changes in pressure can sense sound waves [1], measure changes in height and altitude which is useful for; weather forecasting [2], recognizing out-of-plane orientations [3], and gauging hypersonic flows [4]. Pressure sensors prove very useful in medical applications such as gait analysis, pulse measurement, and blood pressure sensing [5], wearable electronics [6], touch sensing, and a human-skin-like sensor [7]. In preventive maintenance, pressure sensors are used to monitor systems readiness. They monitor tyre pressure [8], aerospace propulsion [9], and pipes for leaks [10]. Different approaches are studied for pressure sensing. Those studies in general aim to obtain a linear relationship between pressure and a value sensed in the range the sensor is required to operate on, and the researchers are looking for the greatest possible sensitivity.

Modern research on pressure sensors is focused on micro-electro-mechanical system (MEMS) technology. With this technology, scientists can manufacture and batch produce highly accurate micro- and nano-features with low cost. Different structures, materials, and physics were investigated to sense pressure. For instance, MEMS technology allows forming a chamber underneath the diaphragm with silicon-to-glass anodic bonding. It is also possible to integrate electronics as field-effected-transistors (FETs) and complementary metal-oxide semiconductors (CMOS) with other structures such as a silicon diaphragm on the same chip [11].

Researchers took advantage of piezoelectric materials' unique properties and used them in pressure sensing [12], the piezoelectric approach was combined with a Wheatstone bridge to linearize pressure-output voltage relation [13]. A cantilever piezoresistor with a variable-size chamber optimize the pressure-frequency response [14]. The main drawback of using piezoelectric material is that it is greatly affected by temperature, which can alter its performance.

Other common methods to measure pressure include an optical technique [15]. Fabry-Perot interferometry was used to establish the relation between pressure and reflection spectrum shift (in nanometers) [15], The principle of interferometry was applied to measure the pressure of acoustic signal with an optical fiber [16]. Using MEMS technology, a Fabry-Perot interferometer was built directly on the optical fiber to sense pressure [17]. One of the drawbacks of using optical sensors is that they are not robust. They are very sensitive, which makes them prone to noise. A better alternative to optical and piezoelectric sensors is capacitive sensors. Capacitive sensors are very sensitive, cost little to make, and require low power; they can be batch fabricated and resist high temperatures [18]. Most capacitive pressure sensors consist of two parallel-plate electrodes separated by a dielectric; capacitance is a function of dimensions, gap, and dielectric material, and such devices

This manuscript is submitted for review on May 30, 2020. The authors would like to acknowledge the financial support of this study by the National Science Foundation (NSF) through grant #CMMI 1919608.

Mohammad Mousavi (smousav1@binghamton.edu), Mohammad Alzgool (malzgoo1@binghamton.edu), and corresponding author, Shahrzad Towfighian (stowfigh@binghamton.edu) are with the Department of Mechanical Engineering in State University of New York at Binghamton.

are tunable with electrostatic excitation [19], [20]. Some of the materials used in capacitive pressure sensors are single-crystal silicon carbide for measurements under very high temperature [21], graphene with graphene oxide as a dielectric [6], dispersed silica for transparency [7], and tunable Young's modulus polydimethylsiloxane [22]. Besides using different materials, different designs can increase sensitivity, examples are placing the sensor in a vacuum to increase its bandwidth [23], or using a simple electronic circuit for analog-to-digital conversion [24]. One downside with the conventional parallel-plate devices is that as the surfaces degrade over time because of repetitive usage, the interaction force gets stronger and can cause permanent failure.

Many researchers have examined the surface interactions for MEMS devices and presented some models to describe them mainly for Atomic Force Microscopes (AFM). The most common model for surface interaction forces is the Lennard-Jones potential (L-J potential) that originates from the atomic interactions between two molecules and consists of a van der Waals attractive component and a repulsive component (also called Paulis effect). According to the results in [25], the attractive force is effective for long distances and the repulsive force is dominant for small gaps. Another surface interaction force is a capillary force because of moisture that might be present between the engaged surfaces . In the MEMS technology, the collapse problem of micro-beams at high humidity environments is a common issue and happens because of capillary forces [26]. Temperature also affects the surface interactions. Assuming a constant meniscus volume, the magnitude of the overall adhesion force decreases with a temperature increase [27]. Increasing the temperature causes the moisture to evaporate, which decreases the adhesion forces. Finally, the elastic recovery of deformed asperities at the contact area is an important cause of the repulsive surface interaction as reported in [28], [29]. The increase of the contact pressure results in the compression of the contact asperities and thereby producing an extra repulsive force at the contact surface.

In this paper, we combine gap-closing and levitation electrodes to provide an easily controlled release mechanism and employ the mechanism for pressure sensing. Previous publications of our group [30], [31] presented an analytical model to describe the electromechanical system behavior and validated it with experiments. Building on our prior work, we elucidate the correlation of the surface interaction forces with the pressure and create a pressure sensor and switch mechanism. We report a comprehensive characterization of the system behavior under two control voltage parameters provided by the gap-closing and levitation electrode systems.

The introduction is followed by a mechanism described in Section II where a pressure sensor and a pressure switching mechanism are described based on the levitation based MEMS and the releasing process. Section III is dedicated to the mathematics of computing the interaction force in the beam equation considering the effects of the bias voltage and pressure. Section IV contains the experimental and analytical results and discussion. Section V concludes this work.

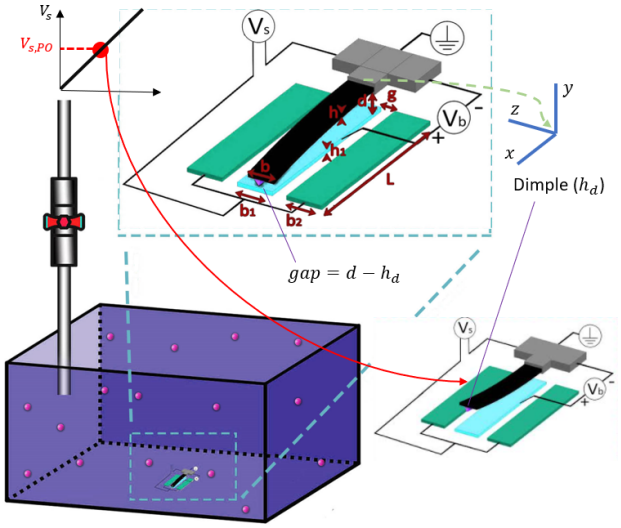

Fig. 1. Schematic of the pressure sensor operation.

II. Mechanism Description

Fig. 1 shows a levitation-based micro-switch [32] that uses a micro-cantilever with a fixed electrode underneath (middle electrode) and fixed electrodes at the sides (two side electrodes). The potential difference between the middle electrode and the micro-cantilever causes the well-known capacitive attractive force. While, charging the side electrodes creates an electrostatic field that drives the micro-cantilever to the opposite direction of the substrate. The side voltage (V_s) and the bias voltage on the middle electrode (V_b) are the tuning parameters of this system.

A. Pressure sensor

The micro-cantilever is initially in pulled-in position. The micro-cantilever is released (pulled-off) by applying a large voltage to the side electrodes, see Fig. 1. Side electrodes create a levitating force that if large enough can overcome the surface forces at the contact area and the capacitive attractive force. The goal of this research is to use a levitation-based micro-switch sensor to measure the pressure inside a chamber or reservoir containing air or other gases. First, the switch micro-cantilever is driven to the pull-in position by applying a sufficiently large V_b. At the pulled-in position, the following forces are applied to the micro-cantilever: restoring force, electrostatic forces (upward and downward), the surface interaction force between the micro-cantilever and the middle electrode, and the reaction force. Applying V_s to the side electrodes generates a levitation force to the pulled-in micro-cantilever. According to our experiments conducted in MEMS and Energy Harvesting Laboratory at Binghamton University, the release process occurs at different side voltages as the pressure varies. We concluded that there is a correlation between the pressure and the release side voltage. Hence, by mapping the measured release side voltage, the chamber pressure is obtained. In this procedure, the pull-off data is used to measure the environmental pressure. The bias voltage

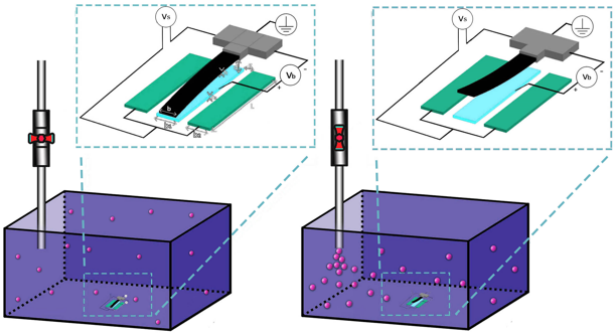

Fig. 2. Schematic of the pressure switch operation.

Symbol	Definition
w	Switch motion $[\mu m]$
f_e	Electrostatic force
$\delta(x)$	Dirac function
f_s	surface interaction force
m	Reduced order equivalent mass
k	Reduced order equivalent stiffness
y	Switch tip displacement
A_j, B_j, β	Electrostatic force coefficients
$V_{b,PI}$	Pull-in bias voltage
L_{eq}	Equivalent beam length

TABLE I
VARIABLES AND PARAMETERS OF THE MATHEMATICAL DESCRIPTION IN SURFACE INTERACTION FORCE SECTION.

V_b is used as a tuning parameter for the purpose of obtaining more linearity.

B. Pressure switch

Consider a chamber that is initially at the pressure of P_0. The chamber inlet is then opened and the inside pressure rises. Our goal is to open a micro-switch as the pressure reaches a specific value P, see Fig 2. As a result of the pressure increase, the surface force of the pulled-in micro-cantilever is reduced. For releasing the switch at the specified pressure P, the tuning parameters V_b and V_s should be selected accordingly. These voltages govern the magnitude of electrostatic force. This device combines pressure sensing and actuation in a single process to make an automatic switch system. It can be applied for gas flow safety systems where the input flow is ceased when the pressure rises to a specified value.

III. SURFACE INTERACTION FORCE FORMULATION

In this section, Newton's second law is used to estimate surface interaction force in pull-in position at the release instant. A mathematical proof that correlates the bias voltage and the pressure with the surface interaction force is provided in the following. The variables and parameters that are used in this paper are introduced in Table. I. The material properties and the switch geometric dimensions can be found in Table. II.

As verified in [33], the Euler-Bernoulli beam model Eq. (1) is considered for the switch micro-cantilever.

Parameter	Symbol	Value
Beam Length	L	$505\ \mu m$
Beam Width	b_3	$20.5\ \mu m$
Beam Thickness	h_3	$2\ \mu m$
Module of Elasticity	E	$160\ GPa$
Density	ρ	$2330\ kg/m^3$
Initial Gap	d	$2\ \mu m$
Bottom Electrode Width	b_2	$32\ \mu m$
Side Electrode Width	b_1	$28\ \mu m$
Electrode Thickness	h_1	$0.5\ \mu m$
Dimple Height	h_d	$0.75\ \mu m$

TABLE II
LEVITATION-BASED MICRO-SWITCH GEOMETRIC DESIGN.

$$\rho A\frac{\partial^2 w}{\partial t^2}+EI\frac{\partial^4 w}{\partial x^4}=f_s(V_b,P)\delta(x-L)+f_e(w,x,t) \quad (1)$$

Using the Galerkin's 1^{st} reduced order approximation, the system partial differential equation turns into a second order ordinary differential equation Eq. (2) where F_{11}: levitating force, F_{12}: interaction between the concurrent electrostatic fields, F_{22}: gap-closing force, f_s: surface interaction force.

$$m\frac{d^2y}{dt^2}+ky=f_s(V_b,P)+F_{11}(y)+F_{12}(y)+F_{22}(y) \quad (2)$$

The electrostatic force model is made up of the side electrodes causing levitating force and the middle electrode causing attractive force as reported in [30]. Considering eqs. (3) to (5), two 9^{th} order polynomials are used for the levitating force and the interaction between F_{11} and F_{22}. A fractional power function models the gap-closing electrode force.

$$F_{11}(y)=V_s^2\sum_{j=0}^{9}A_jy^j \quad (3)$$

$$F_{12}(y)=V_sV_b\sum_{j=0}^{9}B_jy^j \quad (4)$$

$$F_{22}(y)=V_b^2\frac{\beta}{(d+y)^{2.15}} \quad (5)$$

The coefficients A_j and B_j obtained in the interpolating functions have been reported in Table. III. In the pull-in position, the static form of the Eq. (2) should be solved as in Eq. (6) where R is the surface reaction force during the static equilibrium.

$$k(-d+h_d)=F_{11}(-d+h_d)+F_{12}(-d+h_d)+F_{22}(h_d)+f_s+R \quad (6)$$

At the release instant, the reaction force R is vanished, the external forces applied to the micro-cantilever would be the surface interaction force, electrostatic forces and the elastic

Parameter	Value	Parameter	Value
A_0	1.84×10^{-3}	B_0	3.21×10^{-3}
A_1	1.38×10^{-4}	B_1	-2.91×10^{-3}
A_2	1.02×10^{-4}	B_2	9.74×10^{-4}
A_3	1.86×10^{-5}	B_3	-2.55×10^{-4}
A_4	-1.27×10^{-6}	B_4	5.43×10^{-5}
A_5	-1.38×10^{-7}	B_5	-8.52×10^{-6}
A_6	3.70×10^{-9}	B_6	8.97×10^{-7}
A_7	-3.29×10^{-9}	B_7	-5.88×10^{-8}
A_8	1.39×10^{-11}	B_8	2.13×10^{-9}
A_9	-2.31×10^{-12}	B_9	-3.33×10^{-11}
β	-0.463		

TABLE III
THE ELECTROSTATIC FORCE COEFFICIENTS OBTAINED FROM COMSOL DATA.

restoring force. Substituting eqs. (3) to (5) into Eq. (6) gives:

$$k(-d+h_d) = V_s^2 \sum_{j=0}^{9} A_j(-d+h_d)^j + V_s V_b \sum_{j=0}^{9} B_j(-d+h_d)^j + V_b^2 \frac{\beta}{h_d^{2.15}} + f_s \quad (7)$$

There is a constant gap of $d - h_d$ between the parallel electrodes. Let

$$c_{11} = -\sum_{j=0}^{9} A_j(-d+h_d)^j \quad (8)$$

$$c_{12} = -\sum_{j=0}^{9} B_j(-d+h_d)^j \quad (9)$$

$$c_{22} = -\frac{\beta}{h_d^{2.15}} \quad (10)$$

The surface interaction force f_s can be rewritten as

$$f_s = k(-d+h_d) + c_{11}V_s^2 + c_{12}V_sV_b + c_{22}V_b^2 \quad (11)$$

where k is the equivalent stiffness estimated by the reduced order model in Eq. (11) that is identified from experiments for the cantilever beam. The value of k deviates from analytical formulas that assume perfect rigid supports. To account for flexibility in the support, we find an equivalent length, L_{eq}, and thickness, h_{eq} of the beam using the measured natural frequency $f_n = 9650$ kHz and pull-in voltage $V_{b,PI} = 2.05$ V. The measured pull-in voltage for the cantilever beam is a function of beam dimension as explained in [34]:

$$V_{b,PI} = \sqrt{1.72/\alpha_2} \quad (12)$$

where α_2 is a constant defined as:

$$\alpha_2 = \frac{6\epsilon L_{eq}^4}{E h_{eq}^3 d^3} \quad (13)$$

On the other hand, the relationship between the dimensional and non-dimensional natural frequency of a cantilever beam is

$$2\pi f_n = \sqrt{\frac{E h_{eq}^2}{12\rho L_{eq}^4}}\omega_{non} \quad (14)$$

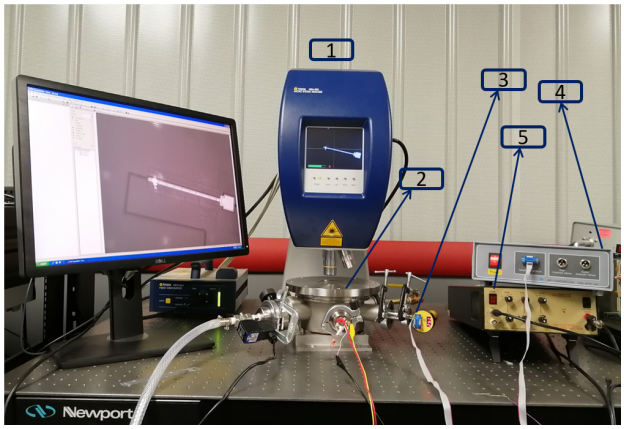

Fig. 3. Experimental setup of the pressure sensor: 1. Laser vibrometer (MSA-500), 2. vacuum chamber, 3. InstruTech pressure sensor, 4. Solenoid controller, and 5. amplifier (Krohn-Hite).

where the nondimensional natural frequency is $\omega_{non} = 3.516$. Two equations Eqs. (13,14) are available with two unknowns h_{eq} and L_{eq}. Substituting the values of Table. II gives $L_{eq} = 533\ \mu m$ and $h_{eq} = 2.015\ \mu m$. The measured values of the beam length and the thickness was reported $505\ \mu m$ and $2\ \mu m$, respectively. The equivalent length account for the flexibility in the support (imperfect boundary conditions). The equivalent stiffness of a cantilever with distributed uniform distributed force is approximated by:

$$k = \frac{8EI}{L_{eq}^3} \quad (15)$$

Using Eq. (15), the equivalent stiffness would be equal to $0.1156\ N/m$.

IV. RESULTS AND DISCUSSION

The experimental setup of the proposed pressure micro-sensor and the pressure-switch is illustrated in Fig. 3. The micro-cantilever with the special electrode design was fabricated using PolyMUMPs standard fabrication performed by MEMSCAP.

All the experiments were conducted at the lab temperature $22°C$, and with the relative humidity of 37 percent. The micro-beam tip displacement and velocity are measured with a laser vibrometer (Polytec MSA-500). The measured data are received and conveyed to MATLAB through a data acquisition system (National Instruments USB 6366 DAQ). The side voltage is provided by a wide-band amplifier (Krohn-Hite 7600). The data acquisition system is also used to provide DC voltage for the middle electrode. The side voltage is approximately 10 orders of magnitude greater than the bias voltage. The disparity is because the electrostatic force caused by side electrodes is based on fringe-field and is weaker than the parallel-plate force caused by the middle electrode. The voltages are manipulated with MATLAB and the outputs are measured and transferred to MATLAB again through the data acquisition system. A sealed chamber was used for low pressures. InstruTech Stinger pressure meter was used to measure the chamber pressure.

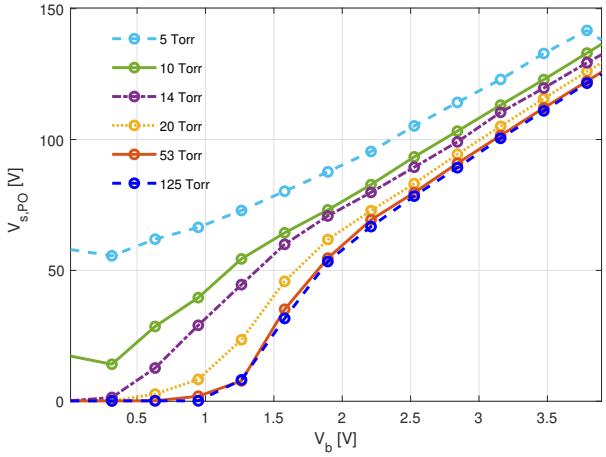

Fig. 4. Switch release side voltage versus bias voltage. The plots were obtained in different pressures shown in the legend.

The release side voltage versus the bias voltage at constant pressures is shown in Fig. 4. At first, the chamber pressure dropped to the values at the legend of Fig. 4, then, the beam is subjected to linear increase of bias voltage (V_b) from $0V$ to $4.5V$ to insure pull-in happens. Then V_b is reduced back to a preset value shown on x-axis in Fig. 4, after fixing that V_b value, linearly increasing side voltage (V_s) from $0V$ to $200V$ is applied to pull-off the beam. The pull-off voltage is recorded on the vertical axis. At pull-off, the downward force, which is the sum of the capacitive and interaction forces, is overcome by the upward forces, which are the levitating and the restoring forces. Therefore, higher bias voltage requires a greater side voltage. Moreover, the comparison of the results of different pressures implies that lower pressures require greater release-side-voltage ($V_{s,PO}$). In other words, for a constant V_b, the surface force is decreased as the pressure rises.

A. Pressure sensor

In this work, V_s is the measuring variable and V_b is considered as a tuning parameter. We could also use V_b as the measurement parameter instead; however, using V_s provides a wide range of voltage variation and therefore we could map the voltage to the chamber pressure with a better resolution.
The release side voltage at the presence of different bias voltages is demonstrated in Fig 5 using the results in Fig. 4. The results show the pressure range of $5\,\text{Torr} < P < 125\,\text{Torr}$. The required release side voltage for the release process is increased as the bias voltage is increased. This plot shows at what driving conditions the micro-switch releases. A linear relation between the $V_{s,PO}$ and the environment pressure is desirable for a pressure sensor. The experimental results show that the operation at greater bias voltages result in more linearity and stability in the range of 5 Torr $< P <$ 20 Torr, See Fig. 5b. Shown by the dashed lines, the linear approximation is also indicated in this figure. Least square was used to find the best lines. Table. IV contains the approximation data as well as the least square error corresponding to each V_b. The best linear fit belongs to the bias voltage of $V_b = 3$ V. The results of testing at higher bias voltages have not been reported

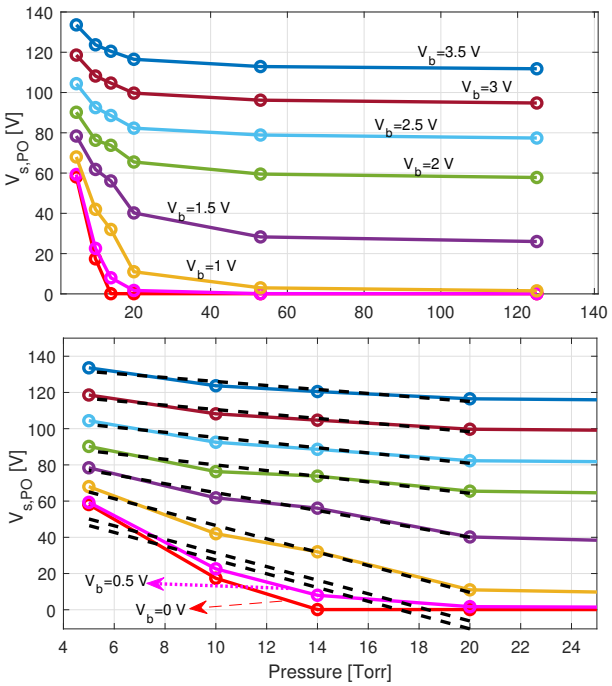

Fig. 5. Switch release side voltage versus the pressure in the presence of constant bias voltages.

because the strong attractive force causes the pulled-in micro-cantilever get permanently stuck.
To show the operation mechanism of the pressure sensor, we chose $V_b = 3$ V, where the most linear relation between P and $V_{s,PO}$ is observed and to make sure the micro-cantilever remains in contact with the bottom electrode ($V_{b,PI} = 2.05$V). The chamber pressure is set to $P = 5$ Torr. Figure 6 shows the time history of the pressure sensing system. Part (a) represents the V_b. Initially, V_b ramps up to make sure that pull-in instability occurs at $t = 0.7$ sec. Then, V_s ramps up until reaching the release side voltage $V_{s,PO}$ and consequently, the micro-cantilever pulls-off (part (b)). At this moment, the levitation force exceeds the surface force and gap-closing force. According to Fig. 5, with $V_b = 3$ V, at $P = 5$ Torr the release side voltage is $V_{s,PO} = 120$ V. By mapping $V_{s,PO}$ to P using the linear approximations indicated in Table. IV, the chamber pressure is estimated at $P = 4.9$ Torr. Using the approximation functions in Table. IV, 2 percent of estimation error is observed in this measurement.

B. Pressure switch

The same device can be used as an automatic switch system detecting when the pressure rises above certain value and opens a safety switch. The two tuning voltage parameters are bias voltage V_b and side voltage V_s. Concerning the choice of the tuning parameter, two practical points are mentioned in the following. Firstly, considering the experimental results shown in Fig. 4, a linear part is suggested at the target pressure P. For example, for switching at $P = 20$ Torr, the tuning parameters are set to $V_b = 3.5$ V and $V_s = 120$ V where a linear relation between the bias voltage and the release side voltage is observed. Secondly, for $V_b < 1$ V, the micro-cantilever is released without applying any side voltage which

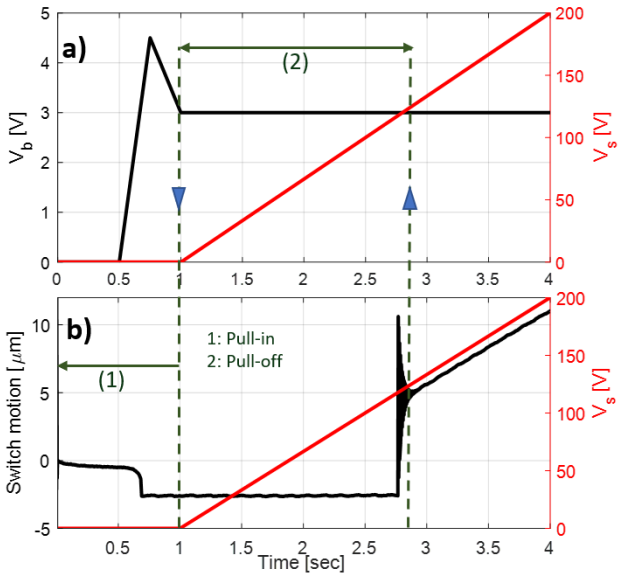

Fig. 6. Time-history of the pressure sensor. Part (a) shows the middle ($\boldsymbol{V_b}$) and side voltages ($\boldsymbol{V_s}$). The switch motion and side voltage are plotted in (b). The operation steps (1) and (2) refer to the pull-in and pull-off process.

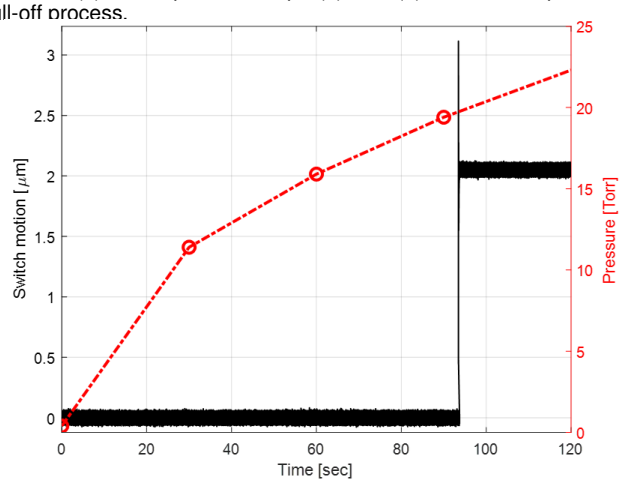

Fig. 7. Pressure switch operation. The black and red plots show the switch motion and chamber pressure versus time, respectively. The tuning parameters are $\boldsymbol{V_b = 3.5}$ V and $\boldsymbol{V_s = 120}$ V

means that this region is not applicable for the pressures higher than 14 Torr. To provide the initial test condition that is the pull-in collapse, V_b should be large enough to hold the micro-cantilever in pull-in position at high pressures. For example, the minimum bias voltage for keeping the beam in pull-in position is $V_b = 1$ V at $P = 125$ Torr. A time-history representing the pressure switch operation is exhibited in Fig. 7. The micro-switch is initially closed. The bias and side voltages are adjusted $V_b = 3.5$ V and $V_s = 120$ V corresponding to release at $P = 20$ Torr. The middle pressure values are approximated, while the pressure of $P = 20$ Torr when the switch opens was measured.

C. Surface interaction force

Using the experimental results, the tuning parameters V_b and V_s at the release instant was measured and reported. The

V_b [V]	a [V/Torr]	b [V]	RMSE [percent/sample]
0	−3.80	65.53	11.15
0.5	−3.75	68.92	8.55
1	−3.69	83.52	2.81
1.5	−2.47	89.32	1.72
2	−1.56	95.61	2.27
2.5	−1.43	109.41	1.88
3	−1.22	122.75	1.73
3.5	−1.10	137.09	1.81

TABLE IV

APPROXIMATION FUNCTION AND ESTIMATION ERROR FOR MAPPING THE MEASURED RELEASE SIDE VOLTAGE TO THE PRESSURE USING THE LINES $\boldsymbol{V_{s,PO} = aP + b}$. THE FORTH COLUMN INDICATES THE ROOT MEAN SQUARE ERROR (RMSE) OF THE APPROXIMATION FUNCTIONS.

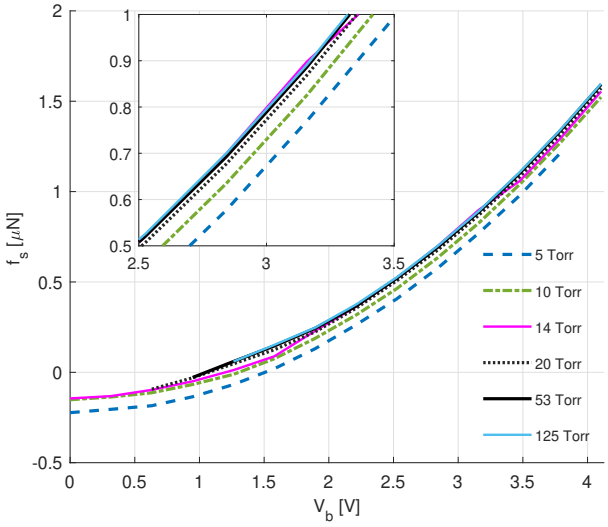

Fig. 8. Surface interaction force of the pulled-in micro-cantilever as a function of the bias voltage at constant pressures.

surface interaction force is calculated using Eq. (11). At a constant pressure, the surface interactions is depicted in Fig. 8. This figure 8 shows at low pressures ($P <\sim 14$ Torr), the surface interaction force is adhesive ($f_s < 0$). At low pressures and zero bias voltage, the micro-cantilever maintains the pull-in position without aiding from the electrostatic force. Considering Figs. 4 at the lowest pressure $P = 5$ Torr, $0.25\mu N$ of surface adhesion force is overcome by the spring force and 60 V of side voltage at the release instant. The interaction force at $P = 10$ Torr is decreased to $0.15\ \mu N$, which indicates the effect of pressure on reducing the adhesion force. At $P = 14$ Torr, the adhesion force and the restoring force cancel each other, and the beam is released at $V_b = 0$ V and $V_s = 0$ V. By applying the bias voltage, the micro-cantilever sticks harder to the bottom electrode. The surface interaction force increases for higher bias voltages (See Fig. 9). The surface interaction force turns into repulsive and pulls away the beam cantilever tip. The calculation of the electrostatic forces and the restoring force shows that the expected release side voltage is noticeably larger than the measured values which reveals the presence of the repulsive interaction force. The transition from adhesive force to repulsive force occurs at 1.5 V for $P = 5$ Torr. For the pressures higher than 14 Torr, there is no adhesion force during the pull-in position. This fact is exhibited in Fig. 8 where the

interaction force is thoroughly positive. For instance, at $P = 125$ Torr, at least $V_b = 1$ V is required for maintaining pull-in and the interaction force is positive for the higher voltages.

To wrap up the discussion about the surface interaction force, we studied the effect of two factors on the interaction forces at the release instant; the bias voltage and pressure. Our observation reveals higher bias voltage or air pressure causes less adhesive and more repulsive interaction force (See Figs. 8 and 9). The increase of bias voltage decreases the effective gap between the beam and the middle electrode. This reduction makes the short-range interaction forces to be dominant, which are of repulsive nature [25]. Our design addresses a major drawback in conventional parallel-plate devices, where releasing from bias voltages well beyond the pull-in voltage is not feasible because the elastic restoring forces cannot overcome the adhesion forces. In the current study, we have used the levitating force as the pull-off mechanism to aid releasing from the substrate. The contact pressure was increased by increasing the middle (bias) voltage. Using the force balance equation, where the only unknown is the net surface force, we observed that the repulsive surface interaction is increased by increasing the bias voltage (contact pressure), see Fig. 8.

We can also explain the effect of ambient pressure on the surface interaction forces. Consider a pulled-in micro-cantilever lying on the lower electrode. Depending on the middle (bias) voltage, the contact pressure between the cantilever tip and the substrate varies. For the middle voltages close to the pull-in voltage, the tip of the pulled-in beam looks like a pin support. By increasing the middle voltage, the pulled-in beam shape converges to the fixed-fixed boundary conditions. As the air pressure increases in this position, the collapsed part of the beam presses more to the substrate (Fig. 10), which causes the effective gap to decrease. This decrease in the gap changes the interaction forces type from long-range to short-range forces, which in this case are going to be repulsive forces (see Fig. 9). Increase of relative humidity can change the type of interaction forces from repulsive to attractive because of the nature of capillary forces. For industrial applications, the mapping of ambient pressure to the release side and bias voltages can be used as a guidance to realize the electronic sensing circuit.

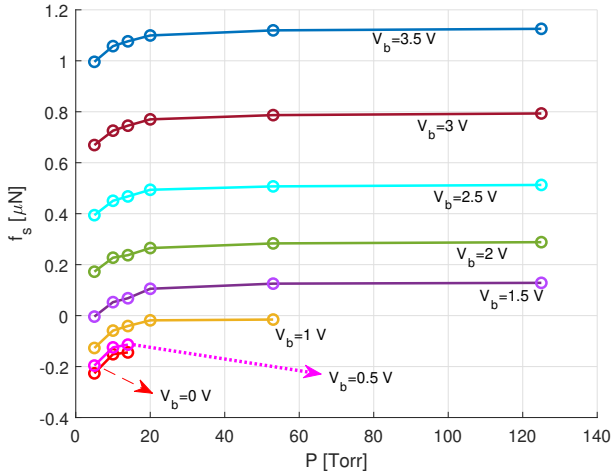

Fig. 9. Surface interaction force of the pulled-in micro-cantilever as a function of the pressure in the presence of constant bias voltages.

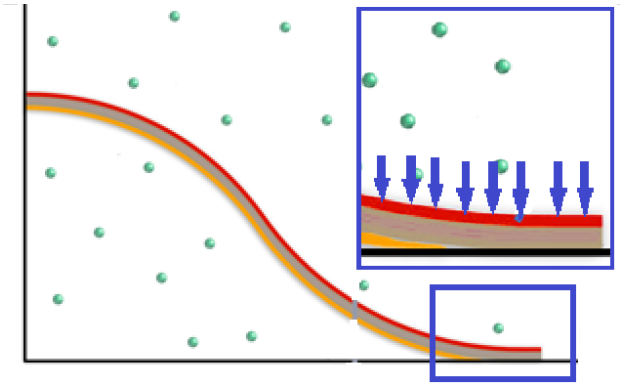

Fig. 10. Beam in the pull-in position and the inset shows the ambient pressure pressing the collapsed part of the beam to the lower electrode. Increase of air pressure reduces the gap distance in the collapsed part of the beam.

V. Conclusion

By merging the electrostatic levitation with the well-known gap-closing MEMS electrodes, we presented a pressure sensor and a pressure switch using the release process. The electrostatic levitation enables the use of the pull-in instability in a wide range of micro-devices. The pressure sensing system considers the gap-closing forces as the tuning parameter and uses the electrostatic levitation force as the measuring variable mapping the side voltage to the environment pressure. A feasibility study for using the pressure sensing idea is proposed and validated. A pressure switch system is also offered in this work. The side and bias voltage as the tuning parameters are adjusted in a way that the switch is released as the pressure reaches a specified value. This levitation-based switch was verified using a laser vibrometer system. For the sake of a reliable and accurate operation, the ideal condition is attaining a linear relation between the driving forces and the environment pressure at the pull-in position. Using the experimental results, we detected the working regions with linear mapping features. The application of electrostatic levitation to MEMS is interesting as it helps the researchers and industry to use a physical phenomenon in micro-scales to investigate the pull-in instability, release, operation range, multi-directional actuation, and control of nonlinearities.

Moreover, using the experimental release measurements of the pulled-in switch at different pressures and different capacitive forces, the surface interaction forces are calculated and reported in this work. The surface interactions are useful for designing MEMS relays and MEMS sensors as the pressure plays a significant role in the operation of micro-scales for designing more reliable devices.

References

[1] J. Voorthuyzen, A. Sprenkels, A. Van Der Donk, P. Scheeper, and P. Bergveld, "Optimization of capactive microphone and pressure sensor performance by capacitor-electrode shaping," *Sensors and Actuators A: Physical*, vol. 26, no. 1-3, pp. 331–336, 1991.

[2] E. Manikandan, K. Karthigeyan, and K. I. A. James, "Micro electro mechanical system (mems) based pressure sensor in barometric altimeter," *International Journal of Scientific & Engineering Research*, vol. 2, no. 8, pp. 1–8, 2011.

[3] S. Zihajehzadeh, T. J. Lee, J. K. Lee, R. Hoskinson, and E. J. Park, "Integration of mems inertial and pressure sensors for vertical trajectory determination," *IEEE transactions on Instrumentation and Measurement*, vol. 64, no. 3, pp. 804–814, 2014.

[4] Y. Seo, D. Kim, and N. A. Hall, "Piezoelectric pressure sensors for hypersonic flow measurements," *Journal of Microelectromechanical Systems*, vol. 28, no. 2, pp. 271–278, 2019.

[5] K. F. Lei, K.-F. Lee, and M.-Y. Lee, "Development of a flexible pdms capacitive pressure sensor for plantar pressure measurement," *Microelectronic Engineering*, vol. 99, pp. 1–5, 2012.

[6] S. Wan, H. Bi, Y. Zhou, X. Xie, S. Su, K. Yin, and L. Sun, "Graphene oxide as high-performance dielectric materials for capacitive pressure sensors," *Carbon*, vol. 114, pp. 209–216, 2017.

[7] H. Kim, G. Kim, T. Kim, S. Lee, D. Kang, M.-S. Hwang, Y. Chae, S. Kang, H. Lee, H.-G. Park *et al.*, "Transparent, flexible, conformal capacitive pressure sensors with nanoparticles," *Small*, vol. 14, no. 8, p. 1703432, 2018.

[8] Z.-H. Zhang, Y.-H. Zhang, L.-T. Liu, and T.-L. Ren, "A novel mems pressure sensor with mosfet on chip," in *SENSORS, 2008 IEEE*, pp. 1564–1567. IEEE, 2008.

[9] P. K. Pattnaik, B. Vijayaaditya, T. Srinivas, and A. Selvarajan, "Optical mems pressure sensor using ring resonator on a circular diaphragm," in *2005 International Conference on MEMS, NANO and Smart Systems*, pp. 277–280. IEEE, 2005.

[10] L. Wong, R. Deo, S. Rathnayaka, B. Shannon, C. Zhang, W. K. Chiu, J. Kodikara, and H. Widyastuti, "Leak detection in water pipes using submersible optical optic-based pressure sensor," *Sensors*, vol. 18, no. 12, p. 4192, 2018.

[11] D. Jang, G. Jung, Y. Jeong, S. Hong, and J.-H. Lee, "Barometric pressure sensor with air pocket integrated with mosfets on the same substrate," *Journal of Semiconductor Technology and Science*, vol. 20, no. 3, pp. 305–310, 2020.

[12] S. S. Kumar and A. Tanwar, "Development of a mems-based barometric pressure sensor for micro air vehicle (mav) altitude measurement," *Microsystem Technologies*, vol. 26, no. 3, pp. 901–912, 2020.

[13] J. W. Song, J.-S. Lee, J.-E. An, and C. G. Park, "Design of a mems piezoresistive differential pressure sensor with small thermal hysteresis for air data modules," *Review of Scientific Instruments*, vol. 86, no. 6, p. 065003, 2015.

[14] R. Wada and H. Takahashi, "Time response characteristics of a highly sensitive barometric pressure change sensor based on mems piezoresistive cantilevers," *Japanese Journal of Applied Physics*, vol. 59, no. 7, p. 070906, 2020.

[15] M. Li, M. Wang, and H. Li, "Optical mems pressure sensor based on fabry-perot interferometry," *Optics Express*, vol. 14, no. 4, pp. 1497–1504, 2006.

[16] X. Wang, B. Li, O. L. Russo, H. T. Roman, K. K. Chin, and K. R. Farmer, "Diaphragm design guidelines and an optical pressure sensor based on mems technique," *Microelectronics journal*, vol. 37, no. 1, pp. 50–56, 2006.

[17] D. C. Abeysinghe, S. Dasgupta, J. T. Boyd, and H. E. Jackson, "A novel mems pressure sensor fabricated on an optical fiber," *IEEE Photonics Technology Letters*, vol. 13, no. 9, pp. 993–995, 2001.

[18] Y. Zhang and K. D. Wise, "A high-accuracy multi-element silicon barometric pressure sensor," in *Proceedings of the International Solid-State Sensors and Actuators Conference-TRANSDUCERS'95*, vol. 1, pp. 608–611. IEEE, 1995.

[19] M. Pallay, R. N. Miles, and S. Towfighian, "A tunable electrostatic mems pressure switch," *IEEE Transactions on Industrial Electronics*, vol. 67, no. 11, pp. 9833–9840, 2019.

[20] H. Zhang, J. Zhong, W. Yuan, J. Yang, and H. Chang, "Ambient pressure drift rejection of mode-localized resonant sensors," in *2017 IEEE 30th International Conference on Micro Electro Mechanical Systems (MEMS)*, pp. 1095–1098. IEEE, 2017.

[21] D. J. Young, J. Du, C. A. Zorman, and W. H. Ko, "High-temperature single-crystal 3c-sic capacitive pressure sensor," *IEEE Sensors Journal*, vol. 4, no. 4, pp. 464–470, 2004.

[22] V. Mitrakos, L. Macintyre, F. C. Denison, P. J. Hands, and M. P. Desmulliez, "Design, manufacture and testing of capacitive pressure sensors for low-pressure measurement ranges," *Micromachines*, vol. 8, no. 2, p. 41, 2017.

[23] A. V. Chavan and K. D. Wise, "Batch-processed vacuum-sealed capacitive pressure sensors," *Journal of Microelectromechanical Systems*, vol. 10, no. 4, pp. 580–588, 2001.

[24] M. Yamada, T. Takebayashi, S. Notoyama, and K. Watanabe, "A switched-capacitor interface for capacitive pressure sensors," *IEEE transactions on instrumentation and measurement*, vol. 41, no. 1, pp. 81–86, 1992.

[25] S. Rützel, S. I. Lee, and A. Raman, "Nonlinear dynamics of atomic–force–microscope probes driven in lennard–jones potentials," *Proceedings of the Royal Society of London. Series A: Mathematical, Physical and Engineering Sciences*, vol. 459, no. 2036, pp. 1925–1948, 2003.

[26] M. De Boer, "Capillary adhesion between elastically hard rough surfaces," *Experimental mechanics*, vol. 47, no. 1, p. 171, 2007.

[27] A. A. Wilson and D. J. Sharar, "Temperature-dependent adhesion mechanisms of metal and insulator probe-sample contact pairs," in *2018 17th IEEE Intersociety Conference on Thermal and Thermomechanical Phenomena in Electronic Systems (ITherm)*, pp. 240–245. IEEE, 2018.

[28] S. J. Timpe and K. Komvopoulos, "An experimental study of sidewall adhesion in microelectromechanical systems," *Journal of microelectromechanical systems*, vol. 14, no. 6, pp. 1356–1363, 2005.

[29] S. J. Timpe and K. Komvopoulos, "The effect of adhesion on the static friction properties of sidewall contact interfaces of microelectromechanical devices," *Journal of microelectromechanical systems*, vol. 15, no. 6, pp. 1612–1621, 2006.

[30] M. Pallay, R. N. Miles, and S. Towfighian, "Merging parallel-plate and levitation actuators to enable linearity and tunability in electrostatic mems," *Journal of Applied Physics*, vol. 126, no. 1, p. 014501, 2019.

[31] M. Mousavi, M. Alzgool, and S. Towfighian, "Electrostatic levitation: an elegant method to control mems switching operation," *Nonlinear Dynamics*, pp. 1–17, 2021.

[32] M. Pallay and S. Towfighian, "A reliable mems switch using electrostatic levitation," *Applied Physics Letters*, vol. 113, no. 22, p. 213102, 2018.

[33] M. Pallay, M. Daeichin, and S. Towfighian, "Dynamic behavior of an electrostatic mems resonator with repulsive actuation," *Nonlinear Dynamics*, vol. 89, no. 2, 2017.

[34] M. I. Younis, *MEMS Linear and Nonlinear Statics and Dynamics*. Springer, New York, 2011.

M ohammad Mousavi received his MSc in Mechanical Engineering from the University of Tehran, Iran in 2017. Since 2019, he has started his PhD in Mechanical Engineering department at Binghamton University. His research interests include simulation, dynamic analysis, and motion control of MEMS sensors and actuators. Triboelectric energy harvesting is his second research area.

M ohammad Alzgool received BSc degree in Biomedical engineering and MS degree in Mechanical engineering from Jordan University of Science and Technology. He has been a PhD student since 2019 in State University of New York at Binghamton since 2019. His areas of interest include MEMS sensors and actuators, modeling, and MEMS fabrication.

S hahrzad Towfighian received her PhD degree in Mechanical Engineering from the University of Waterloo,Canada in 2011. She joined the Mechanical Engineering department at Binghamton University in Fall 2013. Her research interests include Micro-electro-mechanical sensors/actuators and energy harvesting. She develops mathematical modeling of electro-mechanical systems to study nonlinearities and their effect on the system performance. She discovers new ways of sensing and actuation for improving functionality of MEMS devices.